ELSEVIER

Physica C 340 (2000) 16–32

PHYSICA C

www.elsevier.nl/locate/physc

# Structural disorder and superconductivity suppression in $NdBa_2Cu_3O_z$ ($z \sim 7$)

V.V. Petrykin [a,*], E.A. Goodilin [b], J. Hester [d], E.A. Trofimenko [b,c], M. Kakihana [a], N.N. Oleynikov [b], Yu.D. Tretyakov [b]

[a] *Materials and Structures Laboratory, Tokyo Institute of Technology, 4259 Nagatsuta, Midori, Yokohama 226-8503, Japan*

[b] *Inorganic Materials Laboratory, Inorganic Chemistry Division, Chemistry Faculty of the Moscow State University, Lenin Hills, Moscow 119899, Russian Federation*

[c] *Higher College – Faculty of Materials Science of the Moscow State University, Chemistry Faculty, Lenin Hills, Moscow 119899, Russian Federation*

[d] *Australian Nuclear Science and Technology Organisation, New Illawarra Road, Lucas Heights 2234, Australia*

Received 15 July 1999; received in revised form 16 May 2000; accepted 16 May 2000

**Abstract**

Structural features of a low-$T_c$ nearly stoichiometric $Nd_{1+x}Ba_{2-x}Cu_3O_z$ phase ($x \leqslant 0.05$, $z \sim 6.9$, $a = 3.897$–$3.899$ Å, $b = 3.902$–$3.908$ Å, $c = 11.707$–$11.719$ Å) have been investigated for the first time by XRD, EXAFS structure refinement techniques and Raman spectroscopy. It has been found that the abnormal lattice parameters and the low superconductivity transition temperature (55 K) of such a phase are related to structural disorder in the Ba and Nd sites resulting in oxygen disordering which cannot be avoided by a standard oxidation procedure. It is shown that longer annealing at high temperatures is an important factor for reducing the oxygen disordering and hence enhancing superconducting properties after oxidation. 

*PACS:* 74.72.Ny; 74.62.Bf; 81.20.Fw

*Keywords:* $NdBa_2Cu_3O_z$; EXAFS; Raman scattering spectroscopy; Structure refinement; Structural disorder; Superconductivity suppression

## 1. Introduction

The $NdBa_2Cu_3O_z$ superconductor (Nd123) appears destined for wide use in manufacturing bulk materials with enhanced stability of critical current density in high magnetic fields, a higher superconductivity transition temperature ($T_c$) and better chemical stability [1,2]. The commonly accepted advantage of such materials over the classical superconductor $YBa_2Cu_3O_z$ (Y123) is connected directly with an anomalous peak effect caused by nanoscale compositional fluctuations [1–3]. These fluctuations become possible because, unlike the Y123 phase, Nd123 is known to admit a wide range of solid solutions $Nd_{1+x}Ba_{2-x}Cu_3O_z$ (Nd123ss, $x = 0.0$–$1.0$ [4,5]) with superconducting properties suppressed by Nd/Ba heterovalent substitution. This extra degree of freedom in solution demixing probably leads to formation of

* Corresponding author. Tel.: +81-45-924-5310; fax: +81-45-924-5309.

*E-mail address:* valery1@rlem.titech.ac.jp (V.V. Petrykin).

0921-4534/00/$ - see front matter 
PII: S0921-4534(00)00368-3

semicoherent inhomogeneity regions resulting in strong flux pinning [1].

At the same time, it should be noted that the existence of a range of solid solutions makes it more difficult to control the physical properties of materials based on Nd123 since, in addition to the favorable possibility of pinning, some negative side effects may be expected including cation and oxygen disorder in the lattice, which can lead, in general, to "anomalous" samples with suppressed superconducting properties unrecoverable by a complete oxygenation procedure [6]. Such samples of Nd123 phases with low $T_c$ and small orthorhombic distortion are most often ignored or attributed to a form of experimental error (e.g. instrumental error or impurity contamination). In other words, achieving the maximal possible $T_c = 95$ K can be difficult. This problem has been solved partly by application of sophisticated preparation methods such as chemical homogenization of precursors [7–13] followed by a precisely optimized heat treatment [14], melt-solidification under low-$pO_2$ atmosphere [2], or liquid composition control during crystal growth [15–17]. Nevertheless, "anomalous" cases of low-$T_c$ Nd123 phases still remain common, requiring extensive analysis of the underlying causes so that a simple and reproducible method for commercial production can be found.

As the most important specific tasks, searching for preparation conditions followed by structural studies of the "anomalous" samples of Nd123 have to attract special interest because of the consequences that phase transitions and lattice distortions may have on the superconducting properties. Being a transient state to the perfectly ordered Nd123 phase with well-known "ideal" structure, such samples are expected to have local structural deformations rather than long-range changes of their lattice. In this context, extended X-ray absorption fine structure (EXAFS) studies can play a significant role due to the sensitivity of EXAFS to short-range local structure, while Raman scattering spectroscopy brings information about local symmetry and force constants of particular chemical bonds by monitoring the vibrational frequencies and symmetries of observed modes. Both the techniques can examine disorder of light atoms such as oxygen and are complementary to the long-range structure refinement from the X-ray diffraction (XRD) data, which fails to refine oxygen structural parameters adequately and also cannot distinguish Nd and Ba atoms because of their similar scattering factors. Thus, in the present work, we performed a combined study of low-$T_c$ samples of fully oxygenated nearly stoichiometric $Nd_{1+x}Ba_{2-x}Cu_3O_z$ phases by means of XRD, EXAFS, and Raman scattering spectroscopy.

## 2. Experimental

### 2.1. Sample preparation

The $NdBa_2Cu_3O_z$ phase was prepared via two different types of precursors. First, the polymerized complex method [18] was used to obtain highly homogeneous samples. In this method, $Nd_2O_3$ preliminarily annealed at 900°C was dissolved in 20% excess of $HNO_3$. Citric acid and ethylene glycol were added and the solution was stirred at 80°C until it became transparent. Afterwards, stoichiometric amounts of $BaCO_3$ and $Cu_2(OH)_2CO_3$ (with known Cu content) were dissolved in the solution. The temperature was raised up to 140°C and kept constant for 4 h to form a dark-green gel. Finally, the temperature was increased up to 200°C in order to evaporate excess ethylene glycol. The molar ratio of "cation:citric acid:ethylene glycol" in all the experiments was chosen as 1:5:20. The obtained brown polymer was calcinated at 450°C for 5 h, and then annealed in air at 900°C for 15 h. After grinding, the samples were pelletized and sintered in flowing nitrogen gas for 12 and 36 h. Another sample was synthesized using high-quality carbon-free precursors ($Nd_2O_3$, $Ba(NO_3)_2$ and CuO). The substances were mixed in the molar ratio of $NdO_{1.5}$:$Ba(NO_3)_2$:$CuO = 1.05:1.95:3$ and slowly heated in an alumina crucible up to 750°C, then kept at this temperature for 3 h in order to decompose $Ba(NO_3)_2$. The same procedure was repeated with a maximum temperature of 850°C. No interaction with the crucible was observed. After pulverizing the oxide powder in a planetary mill

under acetone, the samples were pelletized, annealed in air on single crystalline MgO substrates at 1000°C for 40 h with one intermediate grinding step, and then quenched into liquid nitrogen. The composition of the sample was slightly shifted ($x = 0.05$) from the ideal ratio 1:2:3 to provide better stability of this ceramic sample at lower temperatures [19]. The small substitution preserves both superconductivity and sample orthorhombicity like in the stoichiometric Nd123 [2,4,5,17], while 2.5 at.% of Nd at Ba sites cannot significantly influence the XRD, EXAFS and Raman scattering spectra.

Oxidation of the samples was performed at 350–400°C in flowing oxygen for 60 h with furnace cooling at the final stage. Such a low temperature allowed, on one hand, the achievement of high oxygen content under high oxygen mobility conditions [1,2,20] and, on the other hand, can prevent possible solid state decomposition of the samples [3].

### 2.2. Characterization

The EDX spectra were collected at about 10 randomly selected grains by Hitachi SEM model S-4500 equipped with an EDS detector and the QUASAR-Kevex Software for X-ray quantitative microanalysis.

Superconducting properties were studied by AC-susceptibility measurements in applied field of 10 Oe at 132 Hz. The real part of the measured signal was used to plot the superconducting transition curves below.

Raman scattering data were obtained by means of a Jobin Yvon/Atago Busan T64000 Raman triple spectrometer equipped with a liquid-nitrogen-cooled CCD detector. An $Ar^+$ laser with a wavelength of 514.5 nm and laser power 20 mW was used for excitation. The spectra were acquired in backscattering geometry at room temperature in air.

X-ray diffraction patterns were collected by a MacScience Diffractometer (CuK$\alpha$ radiation) in the Bragg–Brentano geometry with a step size of 0.02° and acquisition time of 10 s per step. Lattice parameters were estimated by least squares method from XRD patterns taken at 0.5 deg/min using Si as the internal standard.

The crystal structure of the samples was refined by the Rietveld method using the general structure analysis system (GSAS [21]). Raw data were collected in the range of $2\theta = 10°$–$120°$. An initial structural model was set close to the reported Nd123 structure and cation and oxygen positions were refined. The background function was simulated by a Fourier cosine series, and the profile shapes were described employing a multi-term Simpson's rule integration of a pseudo-Voigt function. Preferred orientation of the sample powder and its absorption coefficient were taken into account. Possible disordering between Nd and Ba sites was not considered since both ions have almost equal X-ray scattering factors. The thermal parameters, $B_{iso}$, of the cations were determined after refinement of the atomic positions, where $B_{iso}$ was defined by $T(\theta) = \exp(-B_{iso}\sin\theta^2/\lambda^2)$ [21]. The oxygen thermal parameters were fixed at 1 $\mathring{A}^2$, but the occupation of O1 and O5 sites was allowed to vary within the constraints for the total amount of oxygen determined by iodometric titration.

To measure X-ray absorption spectra, the as-prepared (quenched) or fully oxygenated samples were diluted with boron nitride powder and packed into a circular sample holder 8 mm in radius and 1 mm thick. Dilution factors were chosen to maximize the edge step while maintaining at least 10% transmission at all energies. Actual edge steps ranged from 0.60 to 0.75 of the pre-edge intensity for the Cu edges and from 0.70 to 0.84 for the Nd edges. The sample holder was placed perpendicular to a $2 \times 1$ mm$^2$ monochromatic X-ray beam 15 m downstream from a channel cut by Si 111 monochromator, which was 10.5 m from the bending magnet source of KEK-PF BL-20B (Australian National Beamline Facility) in Tsukuba, Japan, operating at 2.5 GeV with an average current of 300 mA. Harmonic rejection was accomplished by detuning the second face of the monochromator crystal to half (CuK edge) and 60% (Nd LIII edge) of the fully tuned intensity. A 17 cm ionization chamber in front of the sample was used to normalize transmitted intensity measured in the 31 cm post-sample ionization chamber. $N_2$ gas was used in both the chambers at both

energies. Sample transmission data were obtained at the CuK edge and Nd LIII edge. CuK scans extended up to 20 $\text{Å}^{-1}$ from the K edge. The Nd LII edge limited the Nd scans to 11 $\text{Å}^{-1}$. In each case, a 200 eV pre-edge region was scanned in 10 eV steps to enable background subtraction. The post-edge region was scanned in steps of 0.2–0.4 eV. After normalization using monitor counts, background was subtracted using a four-point cubic spline.

Extraction of the extended X-ray absorption fine structure was performed from raw spectra to obtain the data for refinement. This included generally (i) standard preliminary handling of raw X-ray absorption data (normalization, smoothing, background subtraction etc.), (ii) Fourier transform of the spectra and (iii) their windowing to exclude peaks equal or less than 1 Å containing no clear structural information and peaks due to multiple scattering. The range of magnitude of the photoelectron wave vector $k$ for the Fourier transform of all spectra within the Cu-EXAFS or Nd-EXAFS series was fixed at $k = 3$–$16$ $\text{Å}^{-1}$ and $k = 1$–$9.5$ $\text{Å}^{-1}$, respectively. Standard $k$-weighting factor equal to 3 was used. The spectra were filtered using a window in $R$-space (real space) selected from $R = 1.25$–$1.45$ Å to $R = 3.85$–$4.00$ Å (Cu-EXAFS) or from $R = 1.45$–$1.50$ Å to $R = 4.80$–$4.95$ Å (Nd-EXAFS) which includes all the most intensive peaks. In the former case, the upper limit was restricted to be about 5 Å since Y–O2,3-Ba and Y–Cu2–Ba three-body configuration peaks were found for the related $YBa_2Cu_3O_z$ compound at ~5 and ~6.2 Å, respectively [22].

The full-profile refinement procedure of EXAFS spectra and all data processing was done using the XFIT system [23] incorporating the FEFF4 libraries [24] with initial structural values taken from Ref. [25]. In this work, a standard single-scattering approach has been used to obtain a reasonable local structural model of a phase with known structure arrangement rather than to precisely determine the atomic clusters of an unknown compound. For that reason, possible complications like multiple-scattering, double-electron excitation [22,26] etc. were not additionally considered. Therefore, the main structural differences between low-$T_c$ compounds and the conventional (high-$T_c$) Nd123 phase were judged only.

The following parameters were refined for all $n$ selected atomic clusters: $N_i$, $R_i$ and $\sigma_i^2$ ($i = 1, 2, \ldots, n$), where $N$, $R$ and $\sigma^2$ are, respectively, the coordination numbers (the number of back-scattering atoms in shells), average distances (the distance of the atoms in shells from the absorbing atom) and Debye–Waller factors (defined as $T(k) = \exp(-\sigma^2 k^2)$). Additionally the $\sigma^2$ parameters describing the extent of static and dynamic disorder in each shell around the central absorbing atom were restricted to be between 0.001 (ordered shells) and 0.02 $\text{Å}^2$ (disordered shells). Following the need to introduce phase shift correction [23,24], the threshold energy factors $\Delta E_0$ were refined for each spectra (ranged within 0–6 eV). The overall scale factor $S_o^2$ is reported to be 0.85 for similar cuprate compounds [26]; hence, in this paper, it has been fixed at 0.9 in all calculations.

Initial refinement parameters, $N_i$ and $R_i$, were chosen after atomic clusters centered on absorbing atoms (Cu or Nd) have been analyzed. A minimal number of such shells was suggested from the analysis of published reliable diffraction data [25] followed by grouping of the known interatomic distances. It was accepted that a set of distances with slightly different values (<0.1 Å) belongs to one given cluster around an absorbing atom while more diverse sets (>0.1 Å) form other clusters. If this cluster splitting is not carried out, Debye–Waller factors have to cover a large range of distances and will lose their physical meaning due to the atomic displacement distribution no longer being Gaussian. Since the peak width in Fourier-transformed EXAFS spectra introduced by the finite range over $k$ is $\Delta R \sim \pi/k_{max}$ [23,24], expected resolution of the data can be expressed as $\Delta R \geqslant \pi/2k_{max}$, giving, for example, $\Delta R \geqslant 3.14/(2 \times 16) \sim 0.1$ Å for Cu-EXAFS. Therefore, it is reasonable to assume that the shells can be resolved if separated by 0.1 Å. At the same time, coordination numbers in the thus constructed shells should be determined by averaging because XAFS will be the average of contributions from multiple absorbing atom sites in the frame of single-scattering approach [23].

The grouping resulted in usual polyhedra considered in the 123 structure description, so it seems to be both physically reasonable and mathematically justified. During the refinement of such atomic clusters, Debye–Waller factors were refined first within defined restrains followed by refinement of other parameters. Parameter errors were estimated from the least squares values in the final refinement run of a given structural model.

## 3. Results and discussion

### *3.1. Preparation conditions and superconducting properties*

An efficient, if not the only, way to control stoichiometry, impurity levels and compositional uniformity of multicomponent compounds is connected with chemical homogenization. Indeed, soft chemistry methods have been successfully used for mixing of starting materials in order to obtain high-quality single-phase superconducting compounds [13]. In this case, the reaction rate between oxides increases remarkably due to the small grain size of the intermediate fine precursors. At the same time, the rapid preparation of complex cuprates may increase the possibility of their formation in non-equilibrium modifications requiring enormously long oxidation time to reach appropriate values of $T_c$ [8,13]. Therefore, the fundamental possibility remains that such a low-$T_c$ *R*123 represents transient metastable stages interesting from technological and structural points of view.

In our work, pyrolysis of the polymer, obtained after polyesterification at 140°C and oxidation of the remaining organic compounds at 450°C yields a fine mixture of $Nd_2CuO_4$, $BaCO_3$ and CuO with an average particle size of about 100 nm. To enhance the decomposition of barium carbonate, a further calcination was carried out in dynamic vacuum at 800°C. The powder obtained contained a significant amount of $BaCuO_2$, but additional annealing at 900°C in air reduced the intensity of the barium cuprate XRD peaks. Finally, the powder was ground, pressed into pellets and sintered in flowing $N_2$ ($p_{O_2} \approx 10^{-3}$ atm) at 900°C for 12 h, which led to the formation of a single-phase Nd123 sample. Such a single-phase sample exhibited a superconducting transition temperature at $T_c = 55$ K after soaking in pure oxygen at 400°C for as long as 60 h (Fig. 1). (Low-$T_c$ samples can also be prepared in air; studies of the effect of the preparation conditions on sample properties are to be published elsewhere.)

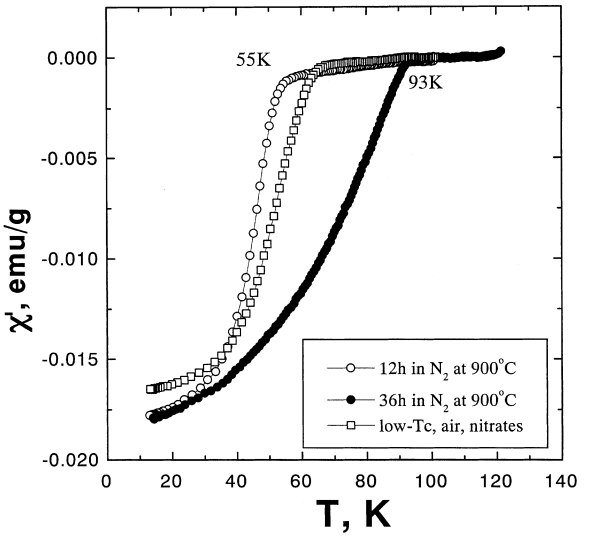


Fig. 1. Superconducting transition temperatures of properly oxygenated $NdBa_2Cu_3O_{\sim 6.9}$ samples prepared by the polymerized complex method (annealing in $N_2$ for 12 and 36 h) and from carbon-free precursors.

Additional annealing in $N_2$ at 900°C for 36 h improved dramatically the sample's $T_c$ after the same oxidation ($T_c$ onset became at 92 K). Note that the oxygen content, which is usually responsible for $T_c$ changes in the $REBa_2Cu_3O_z$ superconductors with fixed cation compositions, in both samples was equal within the titration method error ($z = 6.90$–$6.92$, Table 1). These experimentally determined values ~6.90 would provide proper doping by carriers and, hence, high $T_c$ of the samples as commonly accepted [25]. The results of EDX analysis of both the samples confirmed that the Ba/Nd ratio is close to 2, since Nd:Ba:Cu contents were found to be 0.98(0.04):2.11(0.05): 2.91(0.02) and 0.95(0.03):2.02(0.03):3.03(0.04) in the case of the 12 and 36 h series, respectively, with

Table 1
Lattice constants of $NdBa_2Cu_3O_z$ samples

| Sample | Calculation method | Space group | Lattice constants (Å) | | | Volume (Å$^3$) |
|---|---|---|---|---|---|---|
| | | | $a$ | $b$ | $c/3$ | |
| Oxygenated (exp.) $NdBa_2Cu_3O_{6.90}$ ($N_2$, 900°C, 12 h) | Rietveld | Pmmm | 3.8966(2) | 3.9084(2) | 3.9062(5) | 178.47(2) |
| Oxygenated (exp.) $NdBa_2Cu_3O_{6.92}$ ($N_2$, 900°C, 36 h) | Rietveld | Pmmm | 3.8683(2) | 3.9191(2) | 3.9170(5) | 178.15(1) |
| Quenched (exp.) $Nd_{1.05}Ba_{1.95}Cu_3O_{6.25}$ (air, 1000°C, 40 h) | LSQ | P4/mmm | 3.897(1) | (3.897(1)) | 3.942(1) | 179.60 |
| Oxygenated (exp.) $Nd_{1.05}Ba_{1.95}Cu_3O_{\sim 6.9}$ (air, 1000°C, 40 h) | LSQ<br>Rietveld | Pmmm<br>Pmmm | 3.899(1)<br>3.9018(2) | 3.902(1)<br>3.9021(2) | 3.899(1)<br>3.9026(6) | 177.96<br>178.26(2) |
| Oxygenated $NdBa_2Cu_3O_{6.91}$ [25] | Rietveld | Pmmm | 3.918 | 3.862 | 3.924 | 178.13 |
| $NdBa_2Cu_3O_z$ [5] | Rietveld | Pmmm | 3.919 | 3.868 | 3.917 | 178.13 |
| $Nd_{1.05}Ba_{1.95}Cu_3O_z$ [4] | LSQ | Pmmm | 3.916 | 3.858 | 3.915 | 177.44 |
| Oxygenated [4] | LSQ | Pmmm | 3.888 | 3.883 | 3.891 | 176.23 |
| $Nd_{1.3}Ba_{1.7}Cu_3O_z$ [5] | Rietveld | P4/mmm | 3.891 | (3.891) | 3.887 | 176.55 |
| Oxygenated [4] | LSQ | Pmmm | 3.879 | 3.879 | 3.871 | 174.74 |
| $Nd_{1.5}Ba_{1.5}Cu_3O_z$ [5] | Rietveld | P4/mmm | 3.884 | (3.884) | 3.869 | 175.10 |

statistical errors given in parentheses. Despite a slightly higher standard deviation for the sample with low $T_c$, because of smaller particles and not always perfect orientation of grain surfaces towards the electron beam and EDS detector, the samples are identical within the 0.05 significance level. Thus, such a low $T_c$, a small orthorhombic distortion and a small $c$-constant (~11.72 Å) cannot be explained simply by partial occupation of Ba site by Nd, which indeed results in the decrease of $T_c$ [2,5,16,17].

### 3.2. Structural features studied by X-ray diffraction and Raman spectroscopy

In order to understand these novel features and the reasons of the difference in $T_c$ values of the samples with the same $NdBa_2Cu_3O_{6.90}$ composition, the structure refinement was performed by the Rietveld method using powder XRD data. Results of the structure refinement are presented in Table 2. The observed and simulated XRD patterns and the difference plot are shown in Fig. 2.

The main differences between the refined structures are (i) the altered occupation of oxygen chain sites (Table 2), (ii) displacement or disordering of the apical oxygen as well as (iii) the changes in superconducting and insulating block thickness for the low-$T_c$ sample (Table 3). The high-$T_c$ sample corresponds well to the fully oxygenated ideal Nd123 structure in terms of both the atomic positions [25] and calculated interatomic distances (Table 3). As one may find from the site occupancies and Cu1 thermal parameters, the sample with an initially lower superconducting transition temperature demonstrated stronger disordering in the $CuO_x$ planes, while the sample with the $T_c$ onset around 92 K contains perfectly ordered oxygen chains. It should be noted that the refinement of oxygen occupation parameters from the XRD experiment might be inaccurate, however Raman spectroscopy is known to be sensitive to

Table 2
Fractional coordinates, thermal parameters ($B_{iso}$) and site occupancies refined by the powder XRD Rietveld method for the $NdBa_2Cu_3O_{6.90-6.92}$ samples (see also Table 1) (space group Pmmm (No. 47); thermal parameters of oxygen were fixed at 1 Å$^2$)

| | Oxygenated $NdBa_2Cu_3O_{6.92}$ ($N_2$, 900°C, 36 h) | Oxygenated $NdBa_2Cu_3O_{6.90}$ ($N_2$, 900°C, 12 h) | Oxygenated $Nd_{1.05}Ba_{1.95}Cu_3O_{\sim 6.9}$ (air, 1000°C, 40 h) |
|---|---|---|---|
| $a$ (Å) | 3.8683(2) | 3.8966(2) | 3.9018(2) |
| $b$ (Å) | 3.9191(2) | 3.9084(2) | 3.9021(2) |
| $c$ (Å) | 11.7509(5) | 11.7186(6) | 11.7079(5) |
| Nd(1/2 1/2 1/2), $B_{iso}$ | 0.23(7) | −0.03(6) | 0.01(9) |
| Ba(1/2 1/2 $z$) | | | |
| $Z$ | 0.1821(1) | 0.1822(2) | 0.1825(2) |
| $B_{iso}$ | 1.02(8) | 1.14(7) | 0.17(7) |
| Cu(1) (0 0 0), $B_{iso}$ | 0.79(15) | 1.1(2) | 1.4(2) |
| Cu(2) (0 0 $z$) | | | |
| $Z$ | 0.3511(3) | 0.3527(4) | 0.3479(5) |
| $B_{iso}$ | 0.81(7) | 0.69(7) | 0.16(8) |
| O(1) (0 1/2 0), site occupancy | 0.90(2) | 0.77(5) | 0.51(4) |
| O(2) (0 1/2 $z$), $Z$ | 0.370(1) | 0.374(3) | 0.384(1) |
| O(3) (1/2 0 $z$), $Z$ | 0.370(1) | 0.366(2) | 0.358(2) |
| O(4) ( 0 0 z ), $Z$ | 0.158(1) | 0.162(1) | 0.173(2) |
| O(5) (1/2 0 0), site occupancy | 0.02(2) | 0.13(5) | 0.44(4) |
| $R_{wp}$ (%) | 5.00 | 5.06 | 7.09 |
| $R_p$ (%) | 3.86 | 3.82 | 5.53 |
| $\chi^2$ | 2.035 | 2.549 | 1.979 |

probe oxygen disordering in the Cu1–O1–O5 layer. Fig. 3 displays a good correlation between results of the Rietveld refinement and Raman studies of the oxygenated Nd123 samples.

$NdBa_2Cu_3O_{6.92}$, with a high $T_c$, possessed a Raman spectrum typical for the RE123 compounds. The Raman shift of the apical oxygen mode at 516 cm$^{-1}$ indicates that this specimen is properly oxidized [28]. The broad band at higher frequency corresponds to a possible small degree of disordering in the $CuO_x$ planes. The fully oxygenated sample preliminarily annealed at 900°C for a shorter time ($T_c = 55$ K) exhibits much more significant disordering in O–Cu–O chains. This can be clearly seen from the dramatic increase of the disorder-induced mode at 605 cm$^{-1}$. A break in the O–Cu–O chains and occupation of the O5 site change the local symmetry and result in the appearance of O1 and Cu1 vibrations at 605 and 220 cm$^{-1}$ [29], respectively, which are forbidden in the Raman spectrum of the ideally ordered RE123 structure. Additional signatures of structure distortions in the vicinity of apical oxygen may be found for the low-$T_c$ sample (Fig. 3), particularly, a broad feature at around 575 cm$^{-1}$ normally referred to the IR-active vibrations of apical oxygen [30] and the larger width of the vibration peak of the apical oxygen. The later value in the spectrum of low-$T_c$ sample (52 cm$^{-1}$) is 1.5 times larger than that for the high-$T_c$ sample (35 cm$^{-1}$). It should be mentioned that vibrations of the apical oxygen at 516 cm$^{-1}$ in both the samples indicate that the oxygen concentration is identical. Note, the Raman spectra of the samples do not include peaks caused by impurity phases such as $BaCuO_2$ or $Nd_4Ba_2Cu_2O_{10}$, which have strong Raman active modes at approximately 630 cm$^{-1}$.

The disorder in oxygen chain sites seems to be related to the cation framework, which is ''frozen'' under low-temperature oxygenation conditions but undergoing transformations when it is kinetically allowed at higher temperatures. Our experiments with longer annealing at 900°C in nitrogen resulting in a higher $T_c$ after oxygenation and a smaller degree of disordering in $CuO_x$ planes are in good agreement with the data of Refs. [19,31].

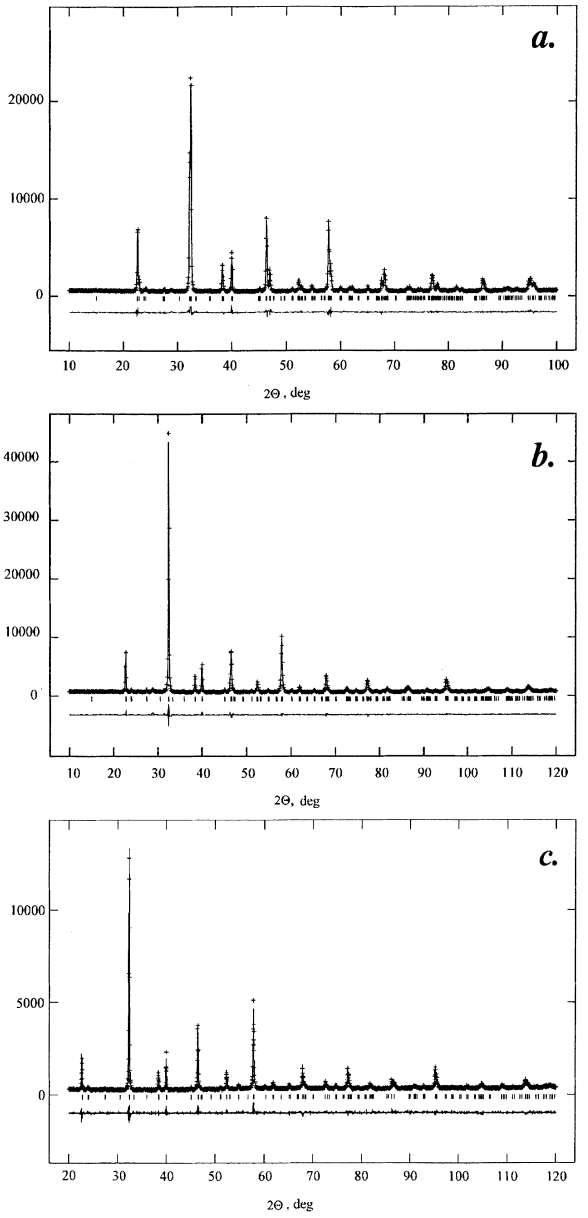


Fig. 2. Experimental diffraction patterns, results of crystal structure refinement by Rietveld method and the difference between the calculated and observed patterns: (a) orthorhombic $NdBa_2Cu_3O_{6.92}$ sample annealed in $N_2$ at 900°C for 36 h and oxygenated, (b) $NdBa_2Cu_3O_{6.90}$ sample annealed in $N_2$ at 900°C for 12 h and oxygenated, (c) $NdBa_2Cu_3O_{\sim 6.9}$ sample annealed in air at 1000°C for 40 h and oxygenated.

These results confirm that in the case of low $pO_2$ the stoichiometric Nd123 phase is stable over a wide range of temperatures [19] and therefore low $pO_2$ and high-temperature annealing can restore the normal (equilibrium) $NdBa_2Cu_3O_z$ structure. At lower temperatures and high-$pO_2$ atmosphere, the unsubstituted Nd123 phase is unstable [19], however high-quality samples and single crystals of the Nd123 phase never demonstrate macroscopic decomposition [3]. In contrast, the obtained disordered tetragonal phase decomposes easily in the solid state under conditions at which reconstruction of the cation skeleton becomes possible (Fig. 4). In this case, an equilibrium solid solution $Nd_{1+x}Ba_{2-x}Cu_3O_{z+y}$ with no defect-induced peaks is formed [4] according to the equation

$$NdBa_2Cu_3O_z + \frac{(y+6x-zx)}{2(1+x)}O_2 \rightarrow \frac{1}{(1+x)}Nd_{1+x}Ba_{2-x}Cu_3O_{z+y} + \frac{3x}{(1+x)}BaCuO_2.$$

Since the oxygen defect-induced peaks in Raman spectrum gradually vanish while the reaction takes place, it can be assumed that disordering in $CuO_x$ planes disappears (Fig. 4) simultaneously with the phase decomposition.

Although the decrease of orthorhombicity, shortening of $c$-axis (and compression of insulation block for the sample prepared from nitrates) are usual for the Nd substitution onto the Ba site, the observed decrease of $T_c$ by 40 K can be hardly explained by a small substitution not detectable by EDS, XRD phase analysis and macro Raman spectroscopy. Additionally, the data in Figs. 3 and 4 and Table 2 demonstrate that stable disordering in the chain site in the obtained tetragonal sample occurs by a different scenario compared to the normal tetragonal $Nd_{1+x}Ba_{2-x}Cu_3O_z$ solid solution with a low $T_c$ since no pronounced defect-induced peaks in the Raman spectra of $Nd_{1+x}Ba_{2-x}Cu_3O_z$ with $x$ as high as 0.4 were observed [30], hence it is obvious that a simple substitution of Nd for Ba, expectable for hypothetical compositional inhomogeneities, cannot explain by itself strong oxygen disordering in the analyzed nearly stoichiometric sample, which would be naturally related to the reducing of $T_c$. One may

Table 3
Selected distances in the atomic clusters/polyhedra around copper and neodymium atoms of the oxygenated compounds $Nd_{1+x}Ba_{2-x}Cu_3O_z$ as refined from XRD data

| Cluster type, central atom–(ligands) | Distances (Å) | | | |
|---|---|---|---|---|
| | Literature data | | Experimental data (Table 2) | |
| | $x = 0.9$[a] [27] | $x = 0$ [24] (set A) | $x = 0$, $z = 6.92$ | $x = 0.05$, $z = 6.90$ (set B) |
| (Cu1–2(O5))[b] | 1.938 | 1.931 | 1.934 | 1.951 |
| Cu1–2(O1) | 2.195 | 1.959 | 1.960 | 1.951 |
| Cu2–2(O3) | 1.939 | 1.947 | 1.947 | 1.954 |
| Cu2–2(O2) | 1.952, 1.957 | 1.975–4 × 1.96 | 1.972–4 × 1.95 | 1.996–4 × 1.96 |
| Cu1–2(O4) | 1.849 | 1.853–2 × 1.85 | 1.857–1 × 1.86 | **2.025** |
| Cu2–1(O4) | 2.198 | 2.266–1 × 2.27 | 2.269–1 × 2.27 | **2.048–2 × 2.04** |
| Cu1–8(Ba) | 3.502 | 3.492–8 × 3.49 | 3.487–8 × 3.49 | 3.490–8 × 3.49 |
| Cu2–4(Ba) | 3.445 | 3.382–4 × 3.38 | 3.395–4 × 3.40 | 3.371–4 × 3.37 |
| Cu2–4(Nd) | 3.21, 3.27, 3.28 ($Nd_{Ba}$) | 3.267–4 × 3.27 | 3.262–4 × 3.26 | 3.284–4 × 3.28 |
| Cu(1,2)–4(Cu(1,2)) | 3.899, 3.87, 3.38, 4.39 | 3.89(3)–4 × 3.89 | 3.89(2)–4 × 3.89 | 3.902–4 × 3.90 |
| Cu(1,2)–2(Cu(2,1)) | 4.025 | 4.119–2 × 4.12 | 4.126–2 × 4.13 | **4.073–2 × 4.07** |
| Cu2–1(Cu2) | 3.458 | 3.534–1 × 3.53 | 3.499–1 × 3.50 | **3.562–1 × 3.56** |
| Nd–8(Cu2) | 3.21, 3.27, 3.28 ($Nd_{Ba}$) | 3.269–8 × 3.27 | 3.262–8 × 3.26 | 3.284–8 × 3.28 |
| Ba–4(Cu1) | 3.502 | 3.492 | 3.487 | 3.490–4 × 3.49[c] |
| Ba–4(Cu2) | 3.445 | 3.382 | 3.395 | 3.371–4 × 3.37[c] |
| Nd/Ba–4(Nd/Ba) | 3.857, 3.608 | 3.89(3)–4 × 3.89 | 3.89(2)–4 × 3.89 | 3.902–4 × 3.90 |
| Nd/Ba–2(Ba/Nd) | 3.751, 3.896 | 3.735–2 × 3.74 | 3.736–2 × 3.74 | 3.717–2 × 3.72 |
| Ba–1(Ba) | 3.864, 4.404 ($Nd_{Ba}$) | 4.301 | 4.280 | 4.273–1 × 4.27[c] |
| Nd–4(O2) | 2.443, 2.472 | 2.454 | 2.464 | **2.377** |
| Nd–4(O3) | 2.476, 2.826 | 2.479–8 × 2.47 | 2.485–8 × 2.47 | **2.563–8 × 2.47**(**9**) |
| Ba–4(O4) | 2.999, 2.527 ($Nd_{Ba}$) | 2.767 | 2.768 | 2.761–4 × 2.76[c] |
| Ba–2(O3) | 3.023 | 2.943 | 2.935 | **2.833** |
| Ba–2(O2) | 2.955, 2.822 ($Nd_{Ba}$) | 2.958 | 2.952 | **3.061–4 × 2.95**(**11**)[c] |
| Ba–2(O1) | 3.080 | 2.909 | 2.902 | **2.893** |
| (Ba–2(O5))[b] | 2.736, 2.664 ($Nd_{Ba}$) | 2.890 | 2.884 | 2.893–4 × 2.89[c] |
| Nd–16(O)[d] | 4.69 | 4.61–16 × 4.61 | 4.60–16 × 4.60 | 4.62–16 × 4.62(5) |
| Nd–8(O)[d] | 4.865 | 4.88–8 × 4.88 | 4.87–8 × 4.87 | 4.72–8 × 4.72 |

[a] Nd ordering in Ba site results in a lager unit cell and more complex coordination. Simplified data without coordination numbers for $Nd_{1.9}Ba_{1.1}Cu_3O_{7.3}$ are listed. ($Nd_{Ba}$) indicates atom in former Ba site.
[b] Occupation of the oxygen position might be close to zero.
[c] Extra shells to be included in calculations if Nd ions occupy these Ba positions.
[d] Second coordination shell.

assume that degradation of $T_c$ in our case may be caused by the synthesis from carbon-rich precursors yielding an oxocarbonate, which decomposes after additional annealing. However, we did not observe a $CO_3^{2-}$ internal mode in the Raman spectrum, the low-$T_c$ sample was prepared also from carbon-free precursors, and the observed structural changes were quite different from those reported for $CO_3$ substituted Y123 [32].

### 3.3. Local distortions probed by EXAFS

The samples prepared either by using nitrates or by polymerized complex method had low $T_c$ (Fig. 1), demonstrated essentially similar lattice constants (Table 1) and possessed quite similar structural parameters (Table 2) which were different from the reported values [4,5,25]. It is unlikely that significant level of alien impurities was present

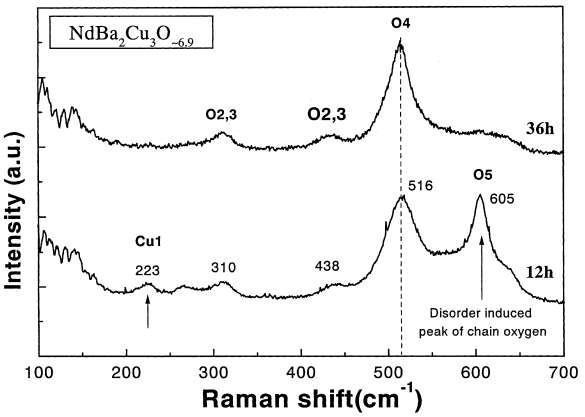


Fig. 3. Macro-Raman spectra of $NdBa_2Cu_3O_{6.90}$ samples annealed in $N_2$ at 900°C for 12 or 36 h and oxygenated.

in the samples. Thus, a small orthorhombicity parameter and low $T_c$ can be independent of preparation method and seems to be caused by similar reasons.

In order to explain the reasons of the disordering in the samples, the short-range local structure and local distortions, rather than the overall long-range structure, was analyzed additionally using X-ray absorption spectra. The reliability was proven by a detailed analysis of statistical errors of structural parameters [26]. A sample prepared from carbon-free precursors as described above was used. The Fourier-transformed spectra of the sample before and after oxygenation are given in Figs. 5 and 6, and Tables 4 and 5 includes results of model refinement.

Phenomenologically, oxygenation keeps Nd-EXAFS – spectra almost unchanged (Fig. 5) except for a slight reduction of peak heights. As expected, Cu-EXAFS Fourier transform spectra

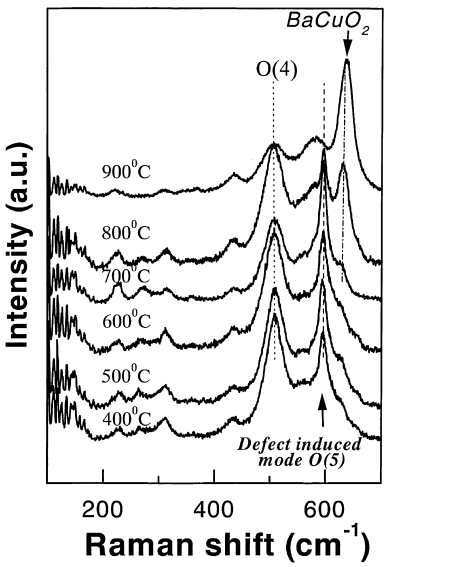


Fig. 4. Decomposition of $NdBa_2Cu_3O_z$ as a result of oxygen annealing for 24 h at the indicated temperatures.

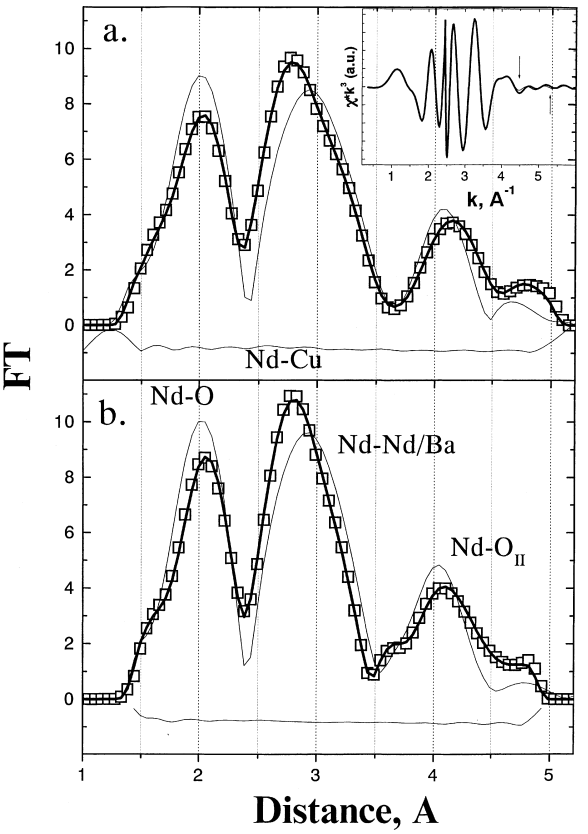


Fig. 5. A windowed Fourier transformation of neodymium X-ray absorption spectra and peak assignment for the low-$T_c$ $Nd_{1.05}Ba_{1.95}Cu_3O_z$ sample after (a) or before (b) its oxygenation. Raw data are given by open squares, a thick line corresponds to the best calculated fitting profile, the difference between the data is given by a line below each spectrum, an assumed spectrum for an ideal Nd123 is presented by a thin line. A typical plot of the observed and calculated $\chi$ values after filtering is given in the insertion, the curves are slightly different at places indicated by arrows. The phase shift correction is not introduced.

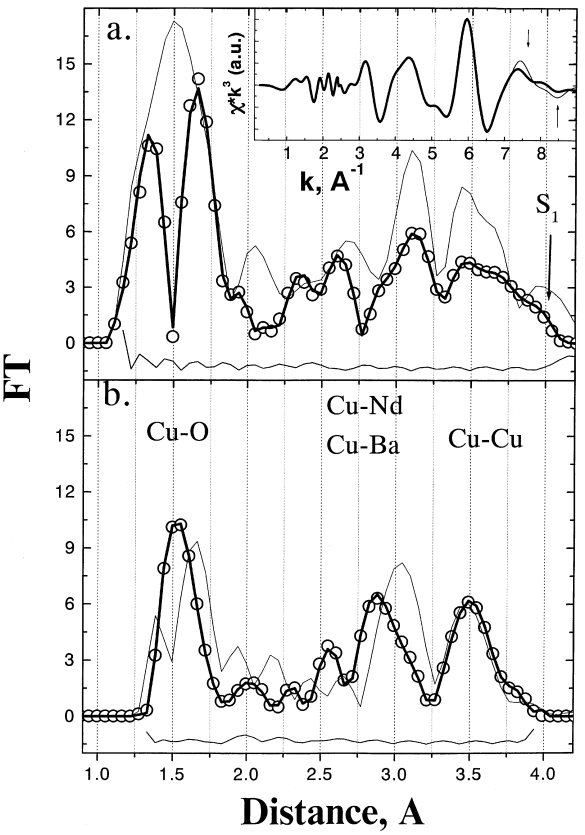


Fig. 6. A windowed Fourier transformation of copper X-ray absorption spectra and peak assignment for the low-$T_c$ $Nd_{1.05}Ba_{1.95}Cu_3O_z$ sample after (a) or before (b) its oxygenation. Raw data are given by open circles, a thick line corresponds to the best calculated fitting profile; the difference between the data is given by a line below each spectrum, an assumed spectrum for an ideal Nd123 is presented by a thin line, $S_1$ – a peak shoulder in the oxygenated sample. A typical plot of the observed and calculated $\chi$ values after filtering is given in the insertion; the curves are slightly different at places indicated by arrows. The phase shift correction is not performed.

of normal sample differ markedly for variable oxygen content, showing changes in peak positions, heights, and width. In Fig. 6, the first group of peaks is associated with in-plane and apical oxygen atoms, the second and the third groups are related to Ba (or Nd) and Cu atoms, respectively. It is obvious that Cu–Nd/Ba as well as Cu–Cu peak heights are slightly lower and that a wide peak shoulder (S1) at about 4 Å is observed for the oxygenated sample, making it possible that metallic shells are unexpectedly more disordered in the fully oxygenated low-$T_c$ phase (Fig. 6a).

Hypothetically, for the ideal Nd123 phase this would be caused by its orthorhombicity, which would give divergent bond lengths for several shells (Table 3). However, in this work, the *a* and *b* parameters were found to be equal for the oxygenated sample (Table 1), therefore the sample is assumed to be tetragonal, at least macroscopically. The only Cu–O peak with reduced height is found for the as-prepared sample (Fig. 6b), hence Cu–O shells have to be more disordered in the quenched sample and contain less oxygen which is, of course, not surprising. The Cu–O FT-peak separation in the case of the oxygenated sample occurs because of the ~0.1 Å difference (Table 3) between corresponding in-plane and apical Cu–O distances. For the quenched sample, however, the only peak of average distance is present.

Unfortunately, to the best of our knowledge, refinement of EXAFS spectra of the particular Nd123 compound is absent in the literature, therefore there is no reference data to compare simplified EXAFS models with a small number of main shells of experimental and known conventional Nd123 compounds. Consequently, such a strategy can demonstrate disorder only in general and cannot reveal meaningful structural changes. Alternatively, for understanding a qualitative picture, it is needed to refine the EXAFS data using a larger number of shells and splitting broad shells into subshells (with the restrictions discussed in Section 2). This makes possible creation of a physically reasonable model and the analysis of changes in "metal (Nd or Cu)–ligand" distances while supplementary information can be taken from Debye–Waller factors under conditions that refined coordination numbers are equal or close enough to structurally expected values in the assumed atomic clusters.

The following preliminary grouping should be accepted (Fig. 7, Table 3) with the atom symbols below given as commonly used [24] (see also Table 2). For the ideal Nd123 structure, it is possible to select a pair of apical O4 oxygen atoms at a shorter distance and a couple of perpendicular O1 chain oxygens at a larger distance from Cu1. Cu2 is surrounded in plane by two pairs of O2 and O3

Table 4
Refined distances ($R$, Å) and Debye–Waller factors (DW, $\times 10^{-3}$ Å$^2$) for the ideal 123 structure model

| Cluster type, absorbing atom–(scattering atom) | As-prepared $Nd_{1.05}Ba_{1.95}Cu_3O_{6.25}$ | | Oxygenated $Nd_{1.05}Ba_{1.95}Cu_3O_{6.90}$ | |
|---|---|---|---|---|
| | Distance $R$ | DW | Distance $R$ | DW |
| Nd–(Nd) | 4.01(7) | 9(12) | 3.99(7) | 6(3) |
| Nd–(Ba) | 3.86(4) | 1(4) | 3.82(4) | 1.0(5) |
| Nd–(Cu) | 3.25(1) | 7(1) | 3.25(1) | 8(1) |
| Nd–(O) | 2.46(1) | 7(2) | 2.44(2) | 9(2) |
| | 4.61(4) | 9(4) | 4.57(5) | 8(4) |
| | 5.26(6) | 3(7) | 4.7(2) | 10(1) |
| ***R***-factor (%) | **23** | | **24** | |
| Cu–(Nd) | 3.18(2) | 6(1) | 3.19(1) | 5(1) |
| Cu–(Ba) | 3.34(3) | 7(1) | 3.32(1) | 3.0(5) |
| | 3.43(2) | 12(1) | 3.47(2) | 9(1) |
| Cu–(Cu) | 3.27(2) | 1.0(5) | 3.62(2) | 1.0(5) |
| | 3.84(2) | 5(1) | 3.96(1) | 4(1) |
| | 4.11(4) | 7(3) | 4.1(2) | 3(1) |
| Cu–(O) | 1.74(4) | 3(3) | 1.73(1) | 1.0(3) |
| | 1.86(1) | 2(1) | 1.93(1) | 6(1) |
| | 2.72(3) | 2(1) | 2.22(2) | 2(1) |
| ***R***-factor (%) | **34** | | **67** | |

oxygens with slightly different Cu–O bonds in the case of an orthorhombic Nd123 phase, and apical oxygen completes the Cu2 coordination pyramid. Therefore, three kinds of averaged bond distances are expected: four atoms with almost same Cu–O distances, a twofold coordinated copper with a short bond Cu1–O4 and a long Cu2–O4 distance since the apical oxygen is shifted from the middle point between the Cu1 and Cu2 atoms (Table 2). Additionally, three different Cu–Cu distances can be found: four Cu2–Cu2 or Cu1–Cu1 in-plane bonds, a shorter Cu2–Cu2 bond in the superconducting block, and a longer Cu1–Cu2 bond in the charge reservoir (Table 3).

The oxygen-free ''Nd-vacancy'' layer sandwiched between two superconducting $CuO_2$ planes is the only perovskite-like block in the structure with equal distances from the central atom: Nd–O and Nd–Cu. In both the cases, the coordination number of Nd has to be 8. The Ba atoms belong to the Ba–O4 layer (Fig. 7) and they are shifted toward the $CuO_2$ plane from the geometrical center of the corresponding perovskite block. As a consequence, two different sets of Ba–Cu distances are present (assumed to be visible in the Cu-EXAFS and invisible in the Nd-EXAFS of ideal 123 phase): shorter Cu2–Ba distances and longer Cu1–Ba ones (Table 3). As for oxygen, Ba is coordinated in-plane by four O4 oxygens, by two O2 and two O3 oxygens above the plane and by some amount of O1 and/or O5 below the Ba–O4 layer. All of these distances cannot be observed in Nd-EXAFS of the ideal 123 phase. It can also be assumed that the Ba–O4 distances are shorter compared to the Ba–O1/O5 distances (Table 3) since the thickness of this block is larger than its in-plane side length. The only Nd–Nd shell is expected to be four Nd atoms in the Nd-layer, however two shorter Nd–Ba and a longer Ba–Ba bonds exist as well (Table 3). The latter, again, should be absent in Nd-EXAFS spectra in the case of ideal Nd123 structure.

At the same time, the shells a priori excluded from the EXAFS of ideal 123 phase, as mentioned above, have to contribute together with all other extra shells (Table 3) in the X-ray absorption spectra if a part of Ba atoms is substituted (or exchanged) by Nd atoms. In these terms, the presence of extra shells has to be most likely

Table 5
Full-profile EXAFS spectra refinement[a] of coordination numbers ($N$), distances ($R$, Å) and Debye–Waller factors (DW, $\times 10^{-3}$ Å$^2$) for shells ($N \times R$, DW) up to 5 Å around a central (absorbing) atom (Nd or Cu) (FEFF4 libraries [22,23])

| Cluster type, absorbing atom–(scattering atom) | As-prepared $Nd_{1.05}Ba_{1.95}Cu_3O_{6.25}$ | Oxygenated $Nd_{1.05}Ba_{1.95}Cu_3O_{\sim 6.9}$ |
|---|---|---|
| Nd–(Nd) | 4(1) × 3.91(2), 2(3)<br>1(3) × 3.6(2), 13(24) | 4(1) × 3.91(3), 6(4)<br>1.0(7) × 3.65(4), 1(7) |
| Nd–(Ba) | 2(1) × 4.39(4), 1(4)<br>8(5) × 3.73(6), 19(11) | 2(1) × 4.37(4), 3(4)<br>7(3) × 3.78(4), 15(8) |
| Nd–(Cu) | 4.2(6) × 3.15(2), 2(1)<br>8.7(9) × 3.30(2), 5(1) | 4.2(6) × 3.16(2), 1(1)<br>8(1) × 3.31(2), 5(1) |
| Nd–(O) | 8(2) × 2.48(3), 12(6)<br>5(3) × 2.68(2), 14(13)<br>3.5(9) × 2.76(1), 1(3)<br>23(10) × 4.51(7), 20(1)[b]<br>9(8) × 5.2(1), 5(11)[b] | 8(2) × 2.46(3), 12(5)<br>5(3) × 2.68(2), 16(13)<br>3(1) × 2.77(2), 5(5)<br>22(10) × 4.53(7), 20(1)[b]<br>11(8) × 5.21(8), 7(9)[b] |
| ***R*-factor (%)** | **4** | **3** |
| Cu–(Nd) | 5(3) × 3.14(5), 16(6)<br>1.2(3) × 3.33(2), 1.0(5) | 4(2)–5(2) × 3.13(3)–3.14(5), 18(2)–20(1)<br>0.9(3)–1.5(6) × 3.31(2)–3.35(3), 2(1)–3(1) |
| Cu–(Ba) | 1.6(3) × 3.23(1), 2.0(5)<br>4(1) × 3.73(1), 3(1) | 1.1(3)–2.0(7) × 3.21(1)–3.22(2), 2(1)–1(1)<br>8(3)–10(5) × 3.76(5)–3.78(4), 11(5)–19(8) |
| Cu–(Cu) | 0.3(5) × 3.66(6), 1.0(5)<br>4(1) × 3.86(1), 3(1)<br>3(1) × 4.25(4), 6(3) | 1.1(3)–1.3(7) × 3.65(3)–3.67(1), 1(1)–5(2)<br>4(1)–5(2) × 3.86(3)–3.90(2), 2(1)–5(3)<br>2.4(7)–2.8(9) × 3.98(2)–4.00(2), 3(2)–3(2) |
| Cu–(O) | <br>3.8(6) × 1.89(1), 5(1)<br>5(3) × 2.37(6), 16(8)<br>1(1) × 2.59(4), 1.0(5)<br>2(1) × 2.72(3), 1.0(5) | 2.1(3)–2.2(3) × 1.75(1)–1.75(1), 1.0(3)–1.0(5)[c]<br>3.0(3)–3.0(3) × 1.92(1), 1.0(3)–1.2(4)<br>3(1)–3(2) × 2.29(3)–2.37(8), 9(4)–18(1)<br>2.0(6) × 2.47(2), 1(1)<br>1.8(6)–1.9(7) × 2.65(2)–2.69(2), 1.0(5)–2(1) |
| ***R*-factor (%)** | **5** | **7**[d] |

[a] LSQ errors are indicated in parentheses, initial sets of parameters are taken from Table 3.
[b] Second coordination shell contributes by these distances in the windowed spectra.
[c] Such short Cu–O distances are reported in a number of works (1.736 Å in $BaCuO_2$ ICDS file #1050, 1.742 Å in $Y_2Ba_4Cu_3O_7$ ICDS file #69260, 1.756 Å in $YBa_2Cu_3O_6$ ICDS file # 63424); however, the value found in the present work may contain errors due to EXAFS FT spectra windowing or multiple scattering effects, therefore this distance is excluded from further consideration.
[d] Parameter ranges are given for the refinements with different initial parameters (modified set A or set B, Table 3), maximum and minimal refined values are listed.

considered as the signature of such substitution. Under these assumptions, the EXAFS local structure refinement permitted reconstruction of the copper and neodymium coordination shells in terms of distances ($R$) to ligands, approximate coordination numbers ($N$), and Debye–Waller factors ($\sigma^2$). Results of several refinement runs are listed in Tables 4 and 5 including an exact 123 model with both coordination numbers and distances fixed at ideal values (Table 3); a model with both refined distances and Debye–Waller factors (Table 4), which keeps unchanged the number of atoms at a given position and their coordination numbers and, finally, the model in which all parameters have been refined (Table 5).

First, it should be noted that the simple model of an ideally ordered Nd123 described above could properly fit none of the spectra. One can see (Figs.

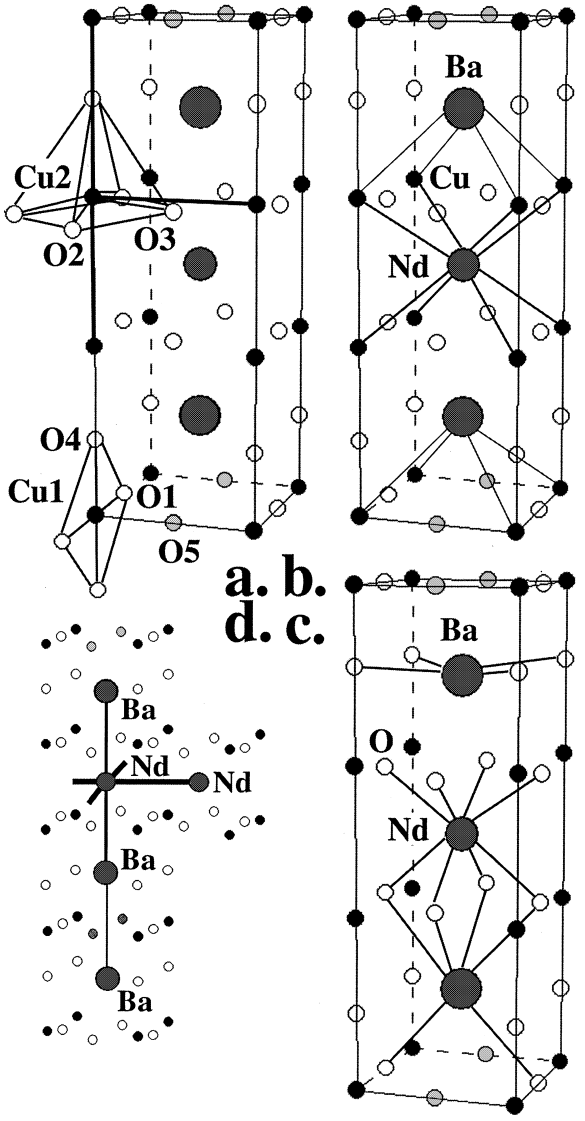


Fig. 7. Crystal structure model of an ideal $NdBa_2Cu_3O_z$ phase and possible coordination polyhedra of Cu, Nd and Ba atoms: (a) Cu–O and Cu–Cu bonds, (b) Nd–Cu and Ba–Cu bonds, (c) Nd–O and Ba–O bonds and (d) Nd–Ba and Ba–Ba bonds.

5 and 6) that peak heights and positions do not match experimental points. *R*-factors as high as ~34% for Nd-EXAFS or even ~123–126% for Cu-EXAFS were observed (intermediate results are not listed in Table 4) if *N* and *R* parameters have been fixed as in the usual Nd123 phase (Table 3). Even if both *R* and $\sigma^2$ parameters are refined, corresponding *R*-factors of about 23–24% and 67–34% are only attainable (Table 4), while the appropriate model (Table 5) gives 3–4% and 5–7% for the Nd- and Cu-EXAFS, respectively. It has to be noted that release of distances values in the refinement of exact 123 model (Table 4) results in the collapse of their mutual consistency while many Debye–Waller factors decrease only insignificantly. Only few distances thus refined can be reasonably interpreted (Table 4). On the other hand, it is impossible to release additionally coordination numbers in the frame of the idealized model since it leads to the loss of physical meaning of the cluster parameters. Therefore, the only way to fit properly experimental EXAFS spectra consists in the consideration that additional shells are present, as discussed above.

The detailed EXAFS refinement with additional shells provides a mathematically stable solution (Table 5) describing structurally a Nd–Ba substitution model related to both 123 and 213 phases (Table 3) which represent terminal points of the $Nd_{1+x}Ba_{2-x}Cu_3O_z$ solid solutions and are characterized by different inter- and intra-layer ordering of Nd and Ba atoms. Most of the distances in Table 5 or their combinations are simply correlated with the lattice constants making it evident that the model is reasonable. For the most interesting oxygenated sample, Nd–Nd and Cu–Cu ("in-plane") distances are approximately equal to the *a* parameter (3.90 Å, Table 1), and the 1.92(1) Å Cu–O bond corresponds to half of this. The sum of the two Cu1–Cu2 and one Cu2–Cu2 ($3.98(2) + 3.98(2) + 3.67(1) \sim 11.65$ Å) or two Nd–Ba and one Ba/Nd–Ba/Nd interlayer distances ($4.37(4) + 3.65(4) + 3.65(4) \sim 11.65$ Å) correlate well with the *c* parameter (11.70 Å, Table 1).

As indicated in Table 5, the EXAFS spectra additionally reflect the presence of a number of extra shells. One can find from the calculation that splitting of the Nd–Cu shell occurs into two subshells with Nd–Cu distances about 3.15 and 3.30 Å. Both distances seem to be real since they are visible in both Nd-EXAFS and Cu-EXAFS spectra. It should be noted that the distances are 0.1 Å longer and 0.05 Å shorter compared to the values of the idealized structure considered above. The same is observed for the Cu–Ba distances

(3.21–3.23 and 3.73–3.76 Å) which are ~0.2 Å shorter and longer than the reported distances. The similar case was found, for example, in the studies of SrK-edge and BaL-edge EXAFS [33] of Sr-substituted $YBa_2Cu_3O_z$, since the local structure in the vicinity of Sr atoms in the Ba-site of Y123 was found to be significantly distorted with four apical oxygen atoms shifted 0.14 Å toward the Sr atoms, and with Sr shifted closer to the Cu2 plane by 0.05 Å. Note that the diffraction techniques demonstrate almost usual atomic positions in the structure in such a case [33,34].

Simultaneously, two extra Nd–Nd distances have to be assumed. The first of them (~3.6–3.65 Å) is ~0.1 Å shorter than the interlayer Nd–Ba distance (observed 3.73–3.78 Å, (Table 5), or expected 3.74–3.76 Å (Table 3)), and the second one (4.37–4.39 Å) is ~0.07 Å longer than the Ba–Ba distance in the ideal structure (Table 3). The shortest Nd–Nd ~3.6 Å and Cu–Cu 3.66 Å distances are not well resolved in the structure of the as-prepared sample, probably because of the larger degree of local distortions expected in the oxygen-deficient sample. XRD data (Table 3) show only a small change of ~0.03 Å of the Ba–Nd and Ba–Ba distances. In addition, two extra Nd–O shells with distances of 2.66–2.68 Å and 2.76–2.77 Å can be found, similar to the Ba–O shells in the ideal Nd123 structure, with the first of them essentially disordered ($\sigma^2 = 0.014$–$0.016$ Å$^2$).

The EXAFS results obtained lead to a conclusion that mixed occupancy of Nd and Ba sites by both $Nd^{3+}$ and $Ba^{2+}$ cations accompanied by a shift from their ideal positions has to be assumed for such a disordered low-$T_c$ Nd123 phase. This idea can be indirectly confirmed by the local change of other distances in the structure found by EXAFS. Oxygenation reduces the longest Cu–Cu distance from almost normal 4.12 Å down to 3.98 Å which is ~0.05–0.1 Å shorter compared to the ideal case. At the same time, the thickness of the superconducting block rises to ~3.66–3.67 Å against the normal value of 3.46–3.53 Å, which is, in general, consistent with the X-ray refinement data (Table 3). This enlargement of the Cu2–Cu2 distance and reduction in the Cu2–Cu1 distance is an evidence for the partial exchange of Ba and Nd between their sites.

Assuming that the $CuO_2$–Nd–$CuO_2$ block thickness is enlarged, a new Nd–O distance as high as ~2.65 Å and a Nd–Cu distance of about ~3.30 Å can be calculated for the Nd atom at the center of this block, which is very similar to the observed values (2.68 and 3.31 Å, respectively, Table 5). At the same time, the observed value of 2.46–2.48 Å for Nd–O indicates that some Nd atoms shift closer to copper (3.15 Å for Nd–Cu). DW-factors are large for this shell since O2 and O3 oxygen atoms have different $z$-coordinates (Table 2). Simultaneously, the distance of 2.77 Å between Nd and oxygens has to be related to the Nd atoms in the former BaO layer in the insulating block (Nd–O4) shifted towards copper and hence introducing another set of short Nd–Cu distances (3.15 Å). Therefore, the Nd–Cu shell displays a large $\sigma^2$ factor (0.016–0.020 Å$^2$). Such a shift has led to local displacement of the apical oxygen and this, indeed, happens since Cu–O apical oxygen distances (2.29 and 2.37 Å) correspond well to the ideal parameters (Table 3) but the $\sigma^2$ factors for them are large. This is consistent with both XRD and Raman spectroscopic data as discussed above.

It should be noted that Nd and Ba atoms remain unsatisfactorily distinguishable by the absorption method although selection of a certain absorbing atom (Nd or Cu) is of course helpful compared to the regular XRD technique. Therefore, refined coordination numbers of Nd–Cu, Cu–Ba and Nd–Nd/Ba shells reflect only roughly the overall features of the Nd and Ba distribution in the structure. In this context, the $S_1$ shoulder (best described by large $N = 10$ and $\sigma^2 = 0.019$ Å$^2$ values for the Cu–Ba shell) of the oxygenated sample and the large coordination number of the 3.73–3.78 Nd–Ba shell (~8) have to be interpreted tentatively as, again, Nd and Ba disorder in the low-$T_c$ phase accompanied, most probably, by displacement of Cu1 which has, according to XRD data (Table 2), 1.5–2 times larger thermal parameters than those in the high-$T_c$ Nd123 phase.

Finally, we ought to note that the EXAFS structural data found for the low-$T_c$ samples, especially Cu–Nd/Ba and Nd/Ba–Nd/Ba distances as well as extra Nd–O bonds, resemble distances in another recently studied compound belonging to the same system, namely the $Nd_2BaCu_3O_z$ phase

[27] (Tables 3 and 5). The salient features of the later phase are conciliated Nd/Ba displacements (Nd–Ba–Nd "waves" [27]), Cu atoms' zig-zag-like shift from ideal positions, and the oxygen lattice rearrangement – everything that was discussed in the case of low-$T_c$ sample. The insulating $CuO_2$–(Nd, Ba)O–$CuO_z$ block architecture of this particular phase seems to be a good approximation for the model of local distortions in the low-$T_c$ Nd123 phase and supports well the idea of Nd atoms' presence in Ba sites. In the $Nd_2BaCu_3O_z$ phase, such distortions reach the long-range scale and become visible by diffraction methods.

The idea of antisite disordering of rare-earth and alkali-earth cations has been proposed but it is still under discussion in the literature. Such an exchange should depend on the difference between rare-earth and alkali-earth ionic radii in the 123-like structure. It is plausible to expect that $Ca^{2+}$ (1.12 Å) can occupy the $Nd^{3+}$ (1.12 Å) site, and $R_{1-x}Ca_xBa_2Cu_3O_z$ compounds exist naturally [35]. In a tetragonal Ba/Sr-substituted Nd123 sample, the authors [34] detected cation disorder between Sr (1.25 Å) and Nd ions and an elongated Cu2–O4 bond which both may be responsible for the lower transition temperature of 71 K.

It is natural to expect that antisite disordering between light rare-earth elements and barium (1.42 Å) would be less probable since the difference between the ionic radii is larger. Nevertheless in a number of papers [4,5,36,37], a slightly negative substitution parameter $x(\mathrm{Ba} \rightarrow \mathrm{Nd})$ is believed to exist although the question is still open. Thus, oxygen disordering in the samples investigated experimentally in the present work seems to be closely related to cation framework antisite disordering, and both coupled phenomena explain the abnormal crystal structure and degradation of superconducting properties.

## 4. Conclusion

In summary, low-$T_c$ "nearly stoichiometric" $Nd_{1+x}Ba_{2-x}Cu_3O_z$ samples ($x \leqslant 0.05$, $z \sim 6.9$, $a =$ 3.897–3.899 Å, $b = 3.902$–$3.908$ Å, $c = 11.697$–11.719 Å) were prepared by the polymerized complex method and from carbon-free precursors. It was found by both XRD and EXAFS structure refinement techniques as well as by Raman scattering that the small orthorhombicity of the samples in a fully oxygenated state and their low superconductivity transition temperature (~55 K) are possibly related to antisite disorder of Ba and Nd accompanied by oxygen disordering which cannot be eliminated by a standard oxidation procedure. It has been shown however that longer duration of annealing at high temperatures is an important factor for reducing oxygen disordering and hence for improvement of superconducting properties after subsequent oxidation.

## Acknowledgements

This work was supported by the Grand-in-Aid for Scientific Research 11450246, RFBR (grant 98-03-32575, 96-15-97385), the Russian Universities Program (grant 98-06-5057) and the Program for Actual Problems of Physics of Condensed Matter (Superconductivity, grant 96079). Part of this work was performed at the Australian National Beamline Facility with support from the Australian Synchrotron Research Program, which is funded by the Commonwealth of Australia under the Major National Research Facilities program. Authors thank V.V. Lennikov (MSU) for measuring the magnetic properties of the experimental samples and G. Foran (ANSTO) for the valuable advice on EXAFS data reduction.

## References

[1] Y. Shiohara, A. Endo, Mater. Sci. Engng. R R19 (1997) 1.
[2] M. Murakami, N. Sakai, T. Higuchi, S.I. Yoo, Supercond. Sci. Technol. 9 (1996) 1015.
[3] M. Nakamura, Y. Yamada, T. Hirayama, Y. Ikuhara, Y. Shiohara, S. Tanaka, Physica C 259 (1996) 295.
[4] E.A. Goodilin, N.N. Oleynikov, G.Yu. Popov, V.A. Shpanchenko, E.V. Antipov, G.V. Balakirev, Yu.D. Tretyakov, Physica C 272 (1996) 65.
[5] K. Osamura, W. Zhang, Z. Metallkd 84 (1993) 522.
[6] K. Jeyabalan, R. Asokamani, S. Natarajan, B. Varghese, J. Solid State Chem. 121 (1996) 415.
[7] S. Shibata, T. Kitagawa, H. Okazaki, T. Kimura, T. Murakami, Jpn. J. Appl. Phys. 27 (1988) L53.

[8] H. Murakami, J. Nishino, S. Yaegashi, Y. Shiohara, J. Ceram. Soc. Jpn. 98 (1991) 624.
[9] P. Krishnaraj, M. Lelovic, N.G. Eror, U. Balachandran, Physica C 215 (1993) 305.
[10] M. Berastegui, M. Kakihana, H. Yoshimura, H. Mazaki, L.-G. Yasuoka, S. Johansson, J. Appl. Phys. 73 (1993) 2424.
[11] A. Sotelo, H. Szillat, P. Majewski, F. Aldeinger, Supercond. Sci. Technol. 10 (1997) 717.
[12] M.R. Palacin, N. Casan-Pastor, P. Gomez-Romero, J. Solid State Chem. 138 (1998) 141.
[13] S. Fujihara, N. Yoshida, T. Kimura, Physica C 276 (1997) 69.
[14] L. Dimesso, M. Marchetta, G. Calestani, A. Migliori, Supercond. Sci. Technol. 10 (1997) 347.
[15] M. Kambara, Y. Watanabe, K. Miyake, A. Endo, K. Murata, J. Mater. Res. 12 (1997) 2873.
[16] G. Krabbes, W. Bieger, P. Schatzle, U. Wiesner, Supercond. Sci. Technol. 11 (1998) 144.
[17] X. Yao, Y. Shiohara, Supercond. Sci. Technol. 10 (1997) 249.
[18] M. Kakihana, J. Sol–Gel Sci. Technol. 6 (1996) 7.
[19] H. Wu, M.J. Kramer, K.W. Dennis, R.W. McCallum, Physica C 290 (1997) 252.
[20] E. Goodilin, M. Limonov, A. Panfilov, N. Khasanova, A. Oka, S. Tajima, Y. Shiohara, Physica C 300 (1998) 250.
[21] A.C. Larson, R.B. Von Dreele, Los Alamos Laboratory Report No LA-UR-86-748, 1987.
[22] J. Rohler, P.W. Loeffen, K. Conder, E. Kaldis, Physica C 282–287 (1997) 182.
[23] P.J. Ellis, H.C. Freeman, J. Synchrotron Rad. 2 (1995) 190.
[24] J. Rehr, J. Mustre de Leon, S.I. Zabinsky, R.C. Albers, J. Am. Chem. Soc. 113 (1991) 5135.
[25] H. Shaked, B.W. Veal, J. Faber, R.L. Hitterman, U. Balachandran, G. Tomlins, H. Shi, L. Morss, P. Paulikas, Phys. Rev. B 41 (1990) 4173.
[26] A. Di Cicco, F. Sperandini, Physica C 258 (1996) 349.
[27] V.V. Petrykin, P. Berastegui, M. Kakihana, Chem. Mater. 11 (1999) 3445.
[28] H.J. Rosen, R.M. Macfarlane, E.M. Engler, V.Y. Lee, R.D. Jacowitz, Phys. Rev. B 38 (1988) 2460.
[29] V.G. Ivanov, M.N. Iliev, Physica C 244 (1996) 333.
[30] R. Nishitani, Y. Yoshida, Y. Sasaki, Y. Nishina, Jpn. J. Appl. Phys. 28 (1989) L569.
[31] M.J. Kramer, A. Karion, K.W. Dennis, J. Electron. Mater. 23 (1994) 1117.
[32] B. Domenges, Ph. Boullay, M. Hervieu, B. Raveau, J. Solid State Chem. 108 (1994) 219.
[33] P. Karen, H. Fjellvag, A. Kjekshus, J. Solid State Chem. 92 (1991) 57.
[34] B. Hellebrand, X.Z. Wang, D. Bauerle, M. Guillaume, P. Fischer, M. Vybornov, P. Rogl, Physica C 261 (1996) 97.
[35] J.P. Zhou, J.-S. Zhou, J.B. Goodenough, J.T. McDevitt, J. Supercond. 8 (1995) 651.
[36] C.T. Lin, A.M. Niraimathi, Y. Yan, K. Peters, H. Bender, Physica C 272 (1996) 285.
[37] N. Watanabe, K. Kuroda, K. Abe, N. Koshizuka, Physica C 300 (1998) 301.